Supporting Information

FeS Decorated Nickel Iron Hydroxide with Regulated Coordination Environment towards Improved Methanol Oxidation Reaction

Xianglong Hu,[a†] Quande Lu,[b†] Xingchen Zhou,[a] Xiaofeng Long,[a] Mengyu Wang,[a] Xueliang Jiang,[a] and Huan Yang,[a,]*

a) Hubei Key Laboratory of Plasma Chemistry and Advanced Materials, School of Materials Science and Engineering, Wuhan Institute of Technology, No. 206 Guanggu 1st Road, Wuhan 430205, China.

b) Shenzhen University, Shenzhen 518055, People's Republic of China.

∗ Corresponding author: H.Y. (Email: yangh@wit.edu.cn).

† These authors contributed equally.

Experimental Methods

Materials and Reagents. Fe foam (99.99%, Aldrich Chemical Co.) used as the substrate. Other reagents and chemicals were analytical reagents (AR) grade. Solutions were prepared with deionized water.

Microbe Cultivation and Inoculation. In this study, sulfate-reducing bacteria (SRB) was isolated from the sludge in Sinopec oilfield, China. SRB seed culture was cultivated in the media (including 0.01 g L^{-1} K_2HPO_4, 0.2 g L^{-1} $MgSO_4 \cdot 7H_2O$, 0.2 g L^{-1} $(NH)_2Fe(SO_4)_2$, 10 g L^{-1} NaCl, 1.0 g L^{-1} Yeast extract, 0.1 g L^{-1} Vitamin C and 4.0 ml L^{-1} Sodium lactate) at 37 ℃. First, the culture medium was treated and sterilized at 121 ℃ for 20 min; next, vials were inoculated with 100 mL of seed culture and 1000 mL of sterile culture, followed by the incubation at 37 ℃. SRB seed culture was obtained after the incubation for 1 day. The initial concentration of SRB inoculum was 8.0×10^4 cells mL^{-1}. The amount of SRB (V_{microbe}) is denoted as the Eq. (1) described:

$$V_{microbe} = \frac{V_{inoculated\ microbe}}{V_{inoculated\ microbe} + V_{sterile\ culture}} \times 100\% \quad (1)$$

Corrosion Electrode Preparation. Iron foam (IF) (2.0×5.0 cm^2) was pretreated in acetone and ethanol (volume ratio is 1:1) for 15 min to remove the electrode surface impurities, then placed into 3 M HCl solution for 1 min to remove the oxide layers on their surface, and rinsed subsequently with water and ethanol, finally dried with nitrogen gas before use. The corrosion electrode was prepared by placing the pretreated IF into a reagent bottle containing 33% (V_{microbe}) SRB, kept in anaerobic environment and incubated at 37 ℃ with different corrosion time (3 days, 7 days and 10 days). Considering the effects of different corrosion environment on the growth of biofilm, different concentration of $NiCl_2$ (0.5, 2.5, 5.1, 30.6 mM) were added into the media. For comparison, blank Fe foam was treated with the sterile medium at 37 ℃ in the same corrosive environment without SRB. After taking out from the SRB corrosion system, the electrodes were rinsed by distilled water and cleaned by absolute ethanol to remove the residual SRB, and dried under a nitrogen gas stream.

Structural Characterization. The morphology of various electrodes was observed with a scanning electron microscope (SEM, JSM-7600F, Japan) and transmission electron microscope (TEM, Tecnai G2 F30, Netherlands). The composition of various electrodes was determined using energy dispersive spectrometer (EDS, Tecnai G2 F30, Netherlands). Raman spectra (HR800, France) were collected at the wavelength of 532 cm^{-1}. The base pressure of x-ray photoelectron spectroscopy (XPS, VG Multilab 2000) analyses in the experimental chamber were below 10^{-9} mbar, the spectra were measured with Al Ka (1486.6 eV) radiation and the overall energy resolution was 0.45 eV and the binding energies were calibrated relative to the C 1s peak at 284.6 eV.

Electrochemical Measurements. The electrochemical tests were performed using an AutoLab 302N potentiostate/galvanostate electrochemical workstation. All the measurements were repeated for at least three times to ensure the reliability of the results. A pretreated electrode used as the working electrode, a graphite rod with relatively large area as the counter electrode and a Hg/HgO electrode as the reference electrode at room temperature (~ 25 ℃). Potentials displayed in this work were converted to the reversible hydrogen electrode (RHE) scale using Eq. (2), and the overpotential $\eta = E_{RHE} - 1.23$.

$$E_{RHE} = E_{Hg/HgO} + 0.0591 \times PH + 0.097 \quad (2)$$

MOR performance testing. The electrolyte used for the test was a 1 M KOH and 1 M MeOH solution with a pH of 14.07. The electrochemical impedance spectroscopy (EIS) was measured at 1.42 V vs RHE. The frequency range was from 10^5 to 0.01 Hz. The linear scan polarization curves (LSV) were measured at a scan rate of 5 mV s^{-1}, starting from 1.0 to 1.6 V vs. RHE. Internal resistance of solution (R_S) of EIS was applied to iR-compensation during LSV tests. CV measurements were performed in the potential range from 1.07 to 1.19 V vs. RHE at different scan rates of 50, 100, 150, 200, 250 mV s^{-1}, and 20 cycles were recorded. The electrochemical surface area (ECSA) of different electrodes was calculated from the CV curve of the twentieth cycle. The stability of the MOR performance of the electrode was tested at constant current densities of 10

mA cm^{-2}.

Computational Methods

DFT Calculations. Spin-polarized DFT calculations were performed using the PBE (Phys. Rev. Lett. 1996, 77, 3865-3868.) functional and the projector augmented wave (PAW) (Phys. Rev. B: Condens. Matter Mater. Phys. 1994, 50, 17953-17979; Phys. Rev. B: Condens. Matter Mater. Phys. 1999, 59, 1758-1775.) potential as implemented in the Vienna Ab Initio Simulation Package (VASP) (Phys. Rev. B: Condens. Matter Mater. Phys. 1996, 54, 11169-11186; Comput. Mater. Sci. 1996, 15-50.). The van der Waals interaction was corrected based on the DFT-D3 scheme (J. Chem. Phys. 2010, 132, 154104.). Given the strong correlation effect of transition metals, DFT + U method was employed with the value of Ueff = 3.8 and 4.3 eV for Ni and Fe atoms (Zhu, B., Dong, B., Wang, F. et al. Unraveling a bifunctional mechanism for methanol-to-formate electro-oxidation on nickel-based hydroxides. Nat Commun 14, 1686 (2023)), ENCUT = 450 eV and EDIFF = 1E-05. All structures in calculations were fully relaxed until the total force on each atom was less than 0.03 eV $Å^{-1}$. The 3 × 1 × 1 k-mesh was employed for the Brillouin zone integrations, and a vacuum layer of 20 Å was used to avoid possible interactions between the slabs. Our catalysts models were built based on $NiFe(OH)_2$ doped FeS atoms. The simplified models had a calculated lattice constant of a = 10.9646 Å, b = 28.9912 Å and c = 23.9906 Å. VASPKIT code (Computer Physics Communications, 2021, 108033.) and VESTA software (J Appl. Crystallogr 2011, 44, 1272-1276.) were used for calculation pre-processing and post-processing.

The adsorption Gibbs free energy (ΔG*) of the adsorbed molecule is calculated as $\Delta G^* = \Delta E + \Delta ZPE - \Delta TS$, where ΔE, ΔZPE and ΔS are the adsorption energy of intermediate reactants in DFT calculation, the correction of zero-point energy and the entropy difference between adsorbed and free molecules, respectively, and the temperature T is set at 298.15 K.

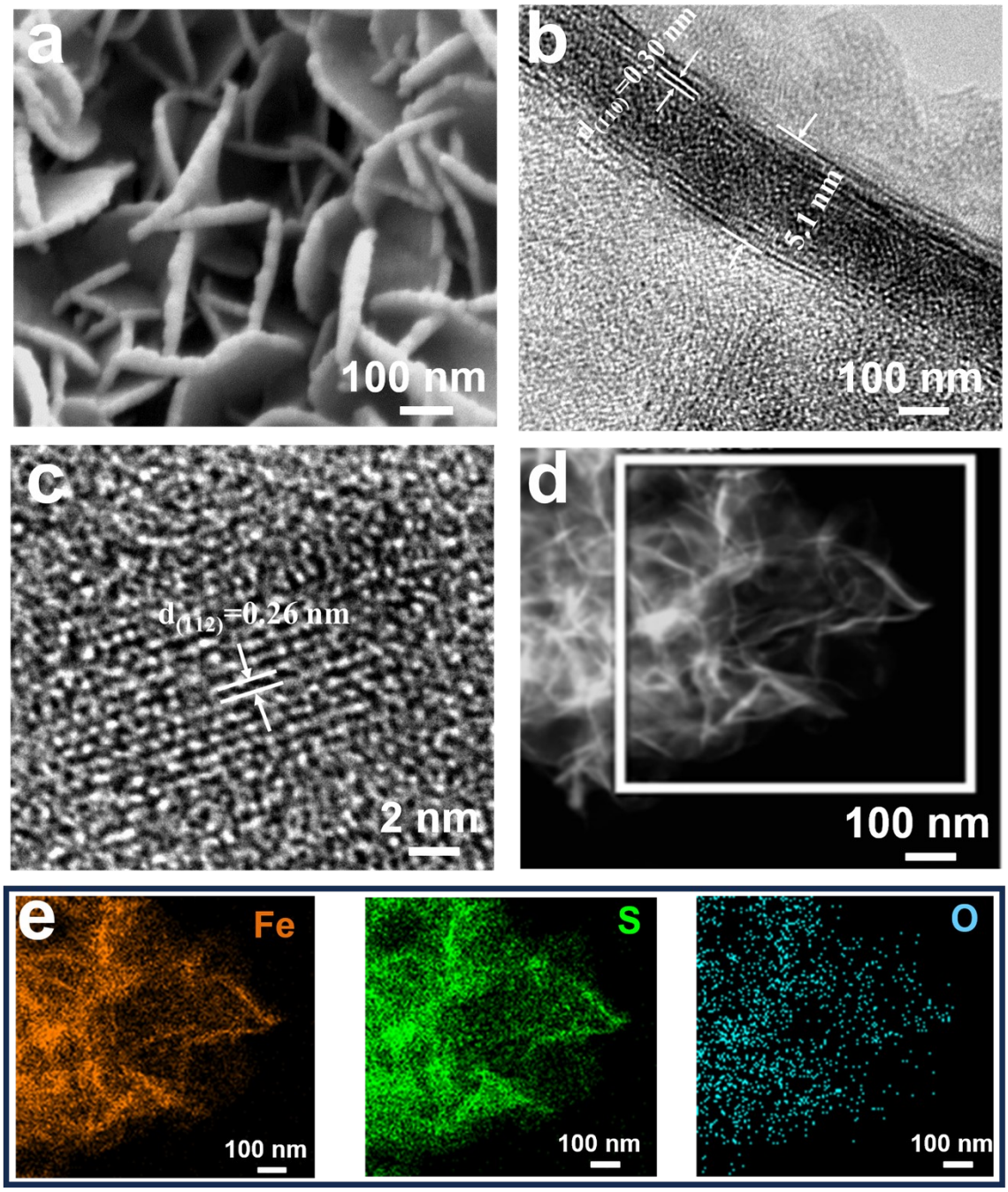

Figure S1. (a) SEM, (b-c) HRTEM images, and (d-e) the corresponding elemental mapping of FeS/IF.

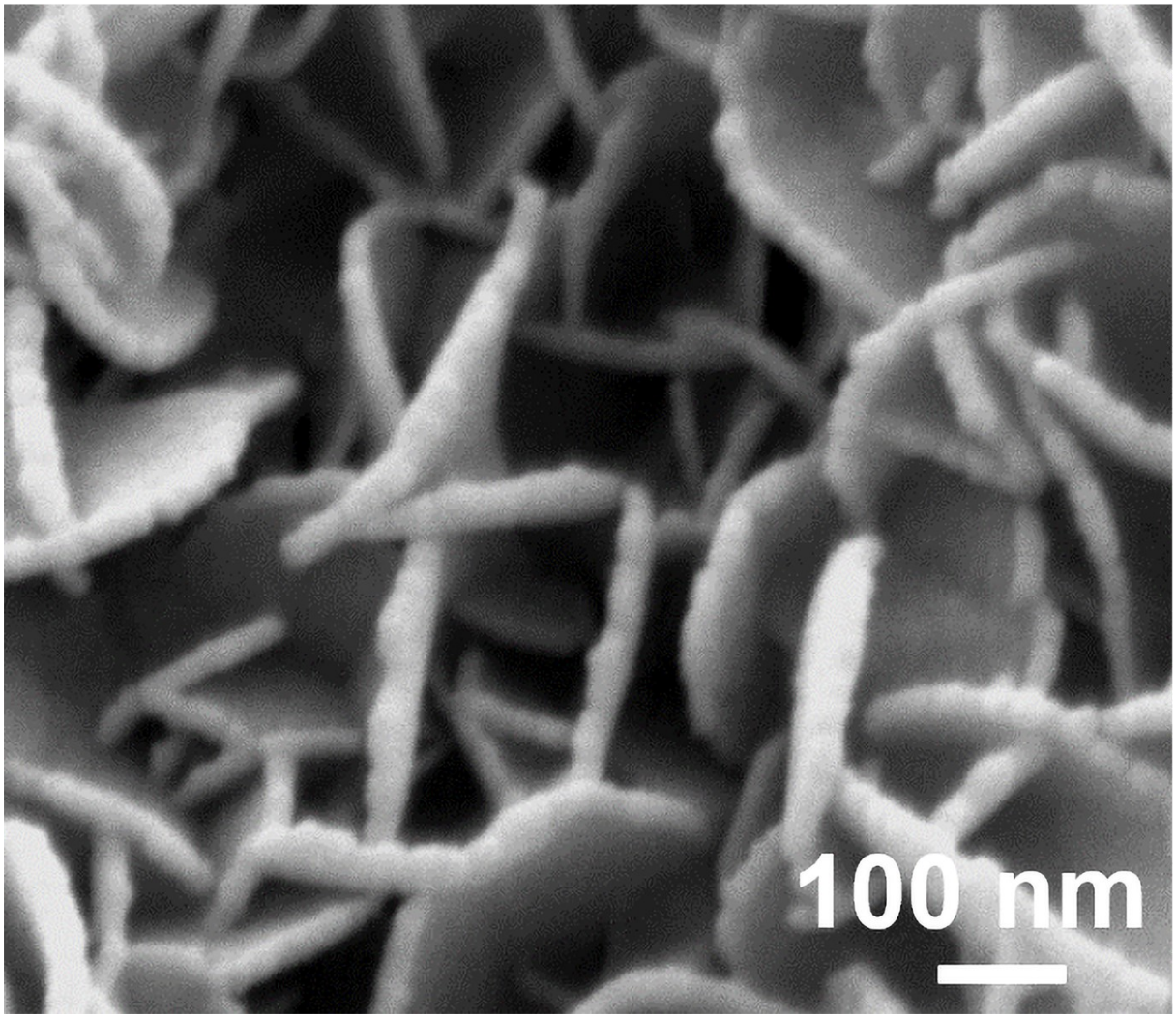

Figure S2. SEM image of $Ni(Fe)(OH)_2$ formed in the absence of SRB.

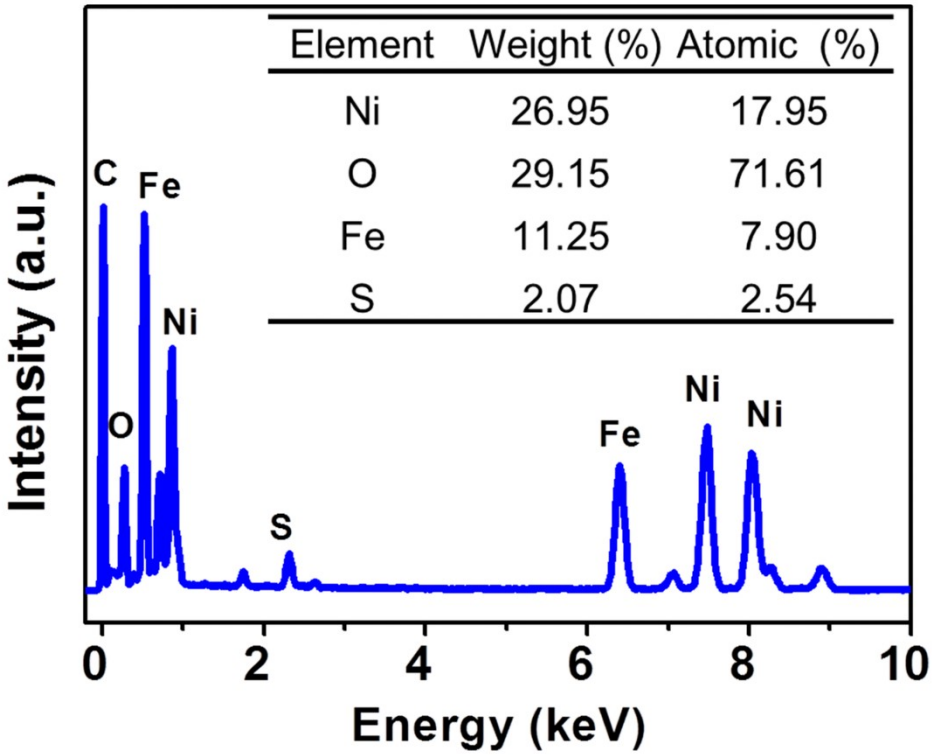

Figure S3. Corresponding EDS profiles of Ni(Fe)$(OH)_2$-FeS in Figure 2e. The inset shows the contents of different elements.

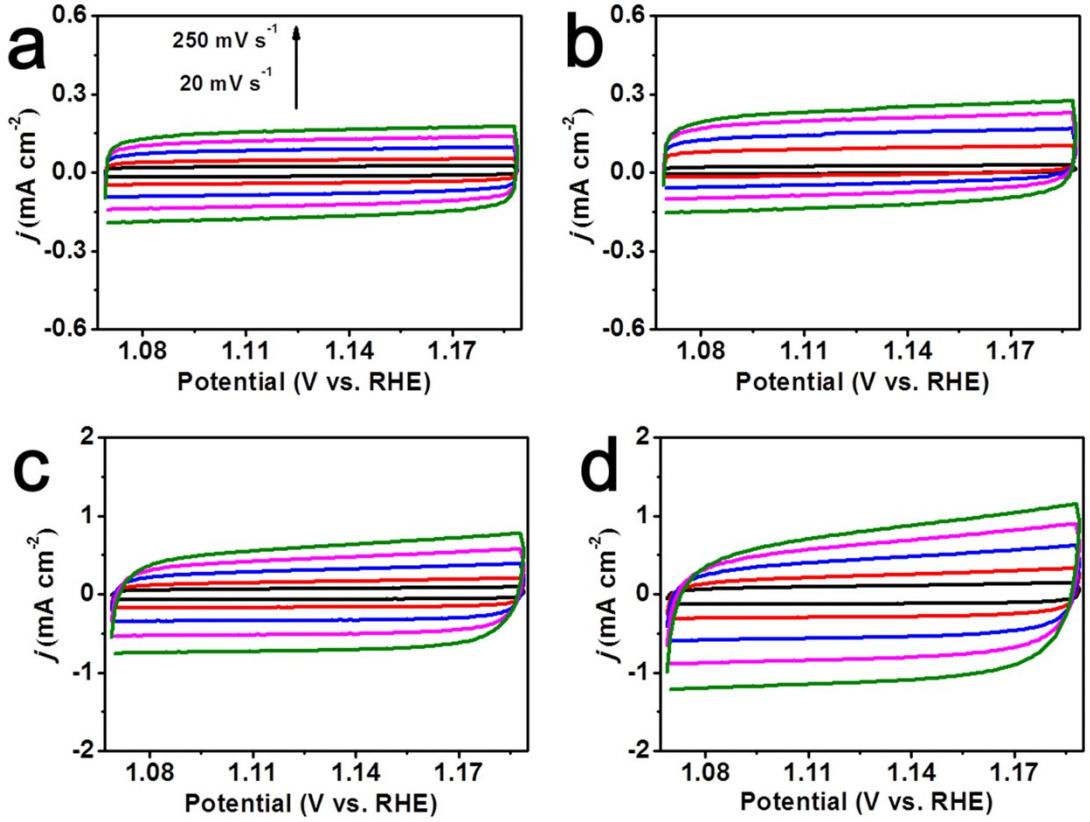

Figure S4. CV profiles of (a) blank IF, (b) FeS/IF, (c) $Ni(Fe)(OH)_2$, and (d) $Ni(Fe)(OH)_2$-FeS electrodes at different scan rates (20, 50, 100, 150, 200 and 250 mV s^{-1}) in MOR.

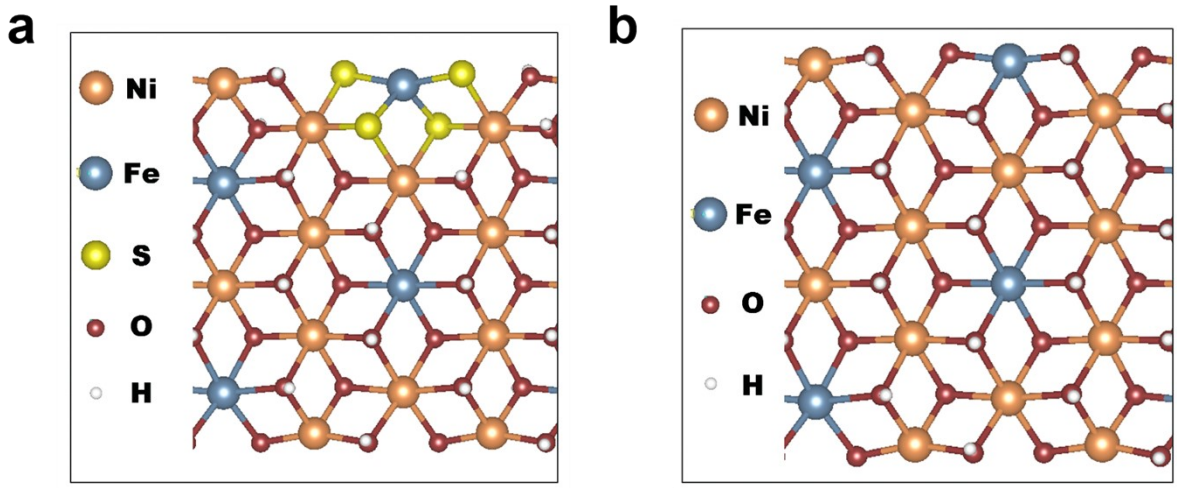

Figure S5. The structures of (a) $Ni(Fe)(OH)_2$-FeS and (b) $Ni(Fe)(OH)_2$.

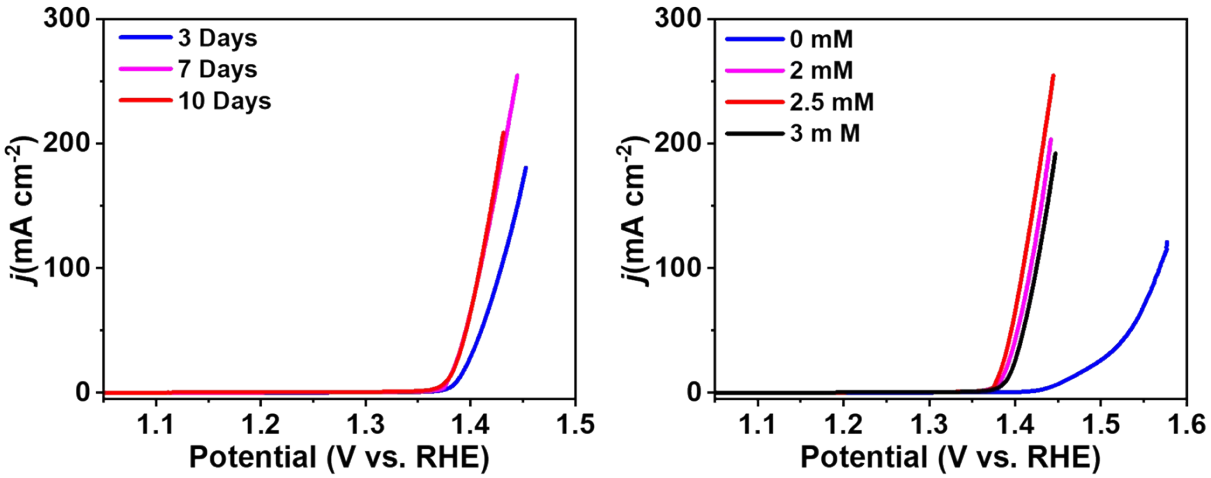

Figure S6. LSV curves of (a) $NiFe(OH)_2$-FeS after 3, 7 and 10 days of corrosion and (b) $NiFe(OH)_2$-FeS in 0, 2, 2.5 and 3 Mm Ni^{2+} concentration of SRB corrosion in 7 days.

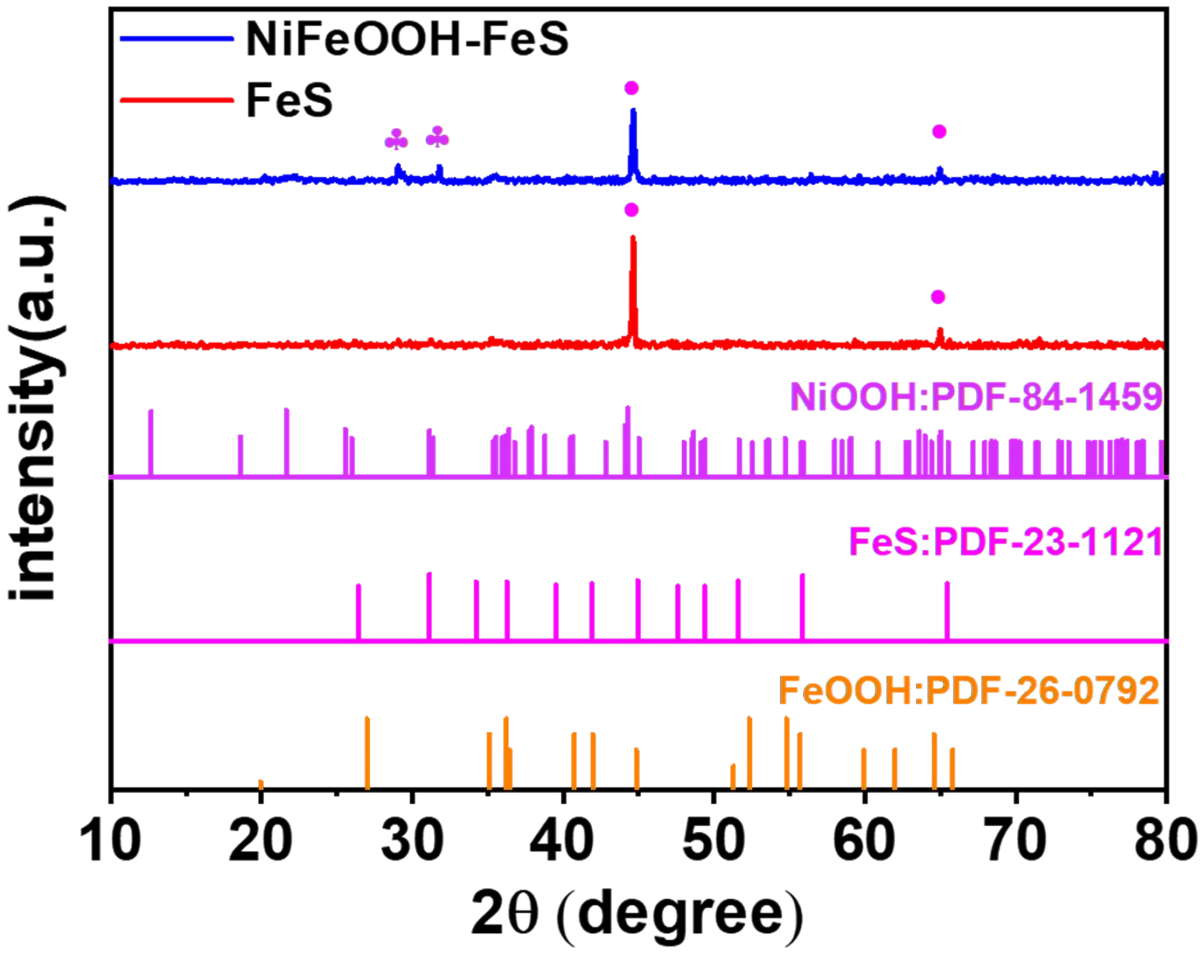

Figure S7. XRD of NiFeOOH-FeS and FeS.

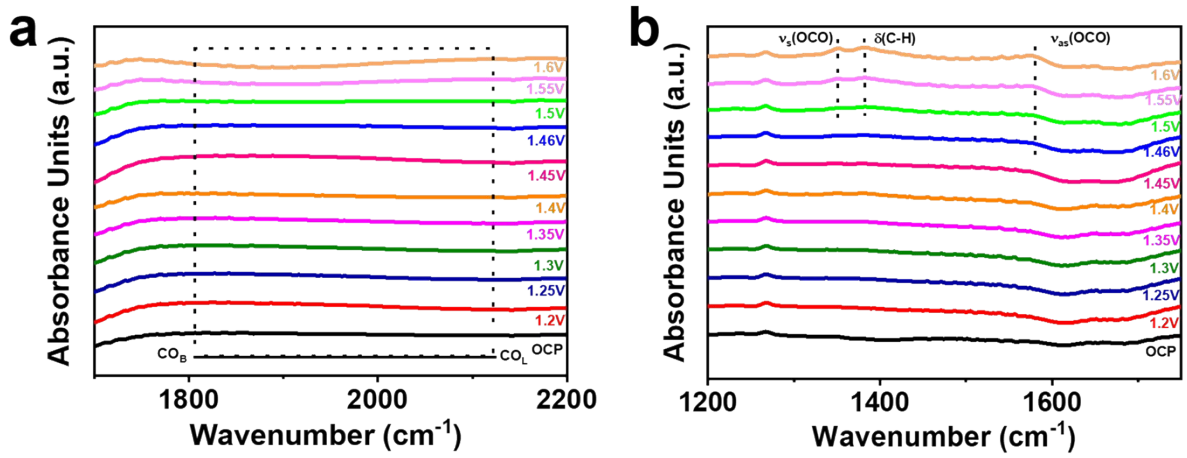

Figure S8. NiFe$(OH)_2$-FeS under various potentials for the 1 M MeOH and KOH in the range of (a) 1700-2200 cm^{-1} and 1200-1750 cm^{-1}.

Table S1. Performance comparison of recently reported NiFe-based MOR electrocatalysts.

Electrode	Synthetic method	Potential at 10 mA cm^{-2}(V vs. RHE)	Tafel slope (mV dec^{-1})	Reference
$Ni(Fe)(OH)_2$-FeS	**Microbial corrosion**	**1.38**	**12**	**This work**
$Cr_{0.02}Ni(OH)_{2+\delta}$	Hydrothermal synthesis	1.39	53	ACS. Catal. **2024**, *14*, 16234-16244.
Ni-SAs/NOMC	Sacrificial template strategy	1.43	-	ACS. Nano. **2025**, *19*, 20001-20011.
Cu−O/OH(Ni)	Potentiostatic anodization	1.42		ACS Appl. Energy Mater. **2022**, *5, 1,* 419–429.
$Ni_{0.75}Fe_{0.25}Se_2$	Two-step solution-based	1.39	54	Small. **2021**, *17*, 2006623.
NiFe-LDH/NiFe-HAB/CF	Electrodeposition	1.41	-	Small. **2023**, *19*, 2208027.
NiFeLDH@SnO_2/NF	Hydrothermal synthesis	1.40	22.4	J. Mater. Sci. Technol. **2022**, *124*, 102-108.
.MoO_3/$Ni(OH)_2$	Magnetron sputtering deposition and electrochemical oxidation	1.39	-	J. Am. Chem. Soc. **2023**, *145*, 26858-26862.
NiIr-MOF/NF	Hydrothermal synthesis	1.41	52.5	Appl. Catal. B-Environ. Energy. **2022**, *300*, 120753.
Ni−Fe_2O_3/O−CNT	Wet chemistry techniques	1.45	54	Chempluschem **2022**, *87*, e202200036.
$LaCo_{0.5}Fe_{0.5}O_3$	Solution-Gelation method	1.56	-	eScience. **2022**, *2*, 87-94.
$Ni(OH)_2$/$MnCO_3$	Hydrothermal synthesis	1.4	54	Chem. Commun. **2024**, *60*, 1591-1594.

NiB-400	Chemical reduction synthesis and annealing	1.39	-	Nat. Commun. **2022**, *13*, 4602.